

Single-bounce quantum gravimeter to measure the free-fall of anti-hydrogen

Joachim Guyomard,^{*} Pierre Cladé,[†] and Serge Reynaud[‡]
*Laboratoire Kastler Brossel, Sorbonne Université, CNRS,
 ENS-Université PSL, Collège de France, 75005 Paris, France*
 (Dated: May 9, 2025)

We introduce an innovative concept for a matter-wave gravimeter, where atoms prepared in a Heisenberg-limited quantum state perform a single bounce on a surface followed by a free fall that reveals interferences. This new approach to quantum gravimetry produces a more robust interference pattern compared to previous multi-bounce proposals. We specify numbers and expected performance for the GBAR experiment, which aims at measuring the free-fall acceleration of antihydrogen at CERN antimatter facilities, and show that this approach improves the expected accuracy of the measurement. Our method opens the door to gravity measurements on rare or exotic atomic species, especially in situations where experimental time or detection events are fundamentally constrained.

As the asymmetry between matter and antimatter in the Universe is one of the fundamental open questions in modern physics, testing the Equivalence Principle on anti-matter remains a key challenge and experimental knowledge is now available with a limited accuracy [1]. The Weak Equivalence Principle [2], that is the universality of free fall independently of the nature and mass of the probe, has been tested with high accuracy on macroscopic matter bodies [3–6] as well as on atoms [7–11]. Ambitious projects are developed at CERN antimatter facilities to measure the free fall acceleration g of anti-hydrogen ($\bar{\text{H}}$) atoms in the gravity field of Earth [12–15]. Among them, the GBAR experiment aims at measuring g at the 1% level by timing the classical free fall of ultracold antihydrogen atoms [16–18].

In this letter we propose to improve this expected accuracy by several orders of magnitude by using a matter-wave interference measurement of the quantum free fall of the atoms rather than timing their classical free fall. The main idea is to let freely falling atoms bounce on a matter surface positioned on their trajectory, due to quantum reflection on the Casimir-Polder interaction when they approach the surface [19–22]. The Casimir-Polder interaction is effective on $\bar{\text{H}}$ as well as on atoms and it should produce quantum reflection and prevent their annihilations on the surface [23–25]. Gravity and reflection produce bound quantum states in the trap they form together, the so-called Gravitational Quantum States (GQS) which have been observed in experiments on ultracold neutrons [26, 27], in which case reflection is produced by repulsive Fermi potential (not by quantum reflection).

In a previous proposal [28] the antihydrogen atoms were supposed to undergo a large number of bounces and thus spend a long time in GQS so that they acquired large phase-shifts for amplitudes corresponding to different states. This implied that the interference pattern had a complex structure (see the Figure 5 in [29]), which contained the information needed to extract the value of g . This complexity appears to be a source of worries since the interference pattern is sensitive to many details to be accounted for in the theoretical calculation of the signal

or its experimental measurement.

The new concept proposed in this letter is a quantum interferometry measurement of free fall, which solves this complexity problem. Matter-wave interferences are now produced for freely falling atoms after a single bounce on a quantum-reflecting surface. The interference pattern has a simple structure discussed below, and leads to a much more direct comparison of theory and experiment. The scheme is completely different from matter-wave interferometers commonly used to measure free fall, where interferences are produced by superpositions of waves having followed different trajectories after beam splitters [30–33]. We will show that the new scheme produces an interferometric measurement of g with a good accuracy, even with a limited sample of detected events.

We will take as an example the application to an improved measurement of g in the GBAR experiment. The accuracy to be expected from the previous proposal was evaluated quantitatively by Monte-Carlo simulations and shown to be better by roughly 3 orders of magnitude in comparison to the classical experiment [28, 29]. Here, we will calculate an even better expected accuracy, though the scheme corresponds to a single bounce rather than many bounces. In these statements, numbers are given for the same resource, that is the same number of $\bar{\text{H}}$ atoms prepared in the same ultracold quantum state,

The schematic representation of the single bounce interferometer is presented on figure 1. The initial state is a Gaussian wave-packet prepared at Heisenberg limit in a trap. In GBAR, $\bar{\text{H}}^+$ ions are prepared in the ground state of an ion trap and $\bar{\text{H}}$ neutral atoms are then obtained by photodetaching the excess positron [34]. The laser pulse used for the photodetachment is used as the Start signal of a time-of-flight measurement with the Stop signal given by annihilation on the detection plate. As the horizontal distance D from the source to the detection plate is fixed (and the size of the source negligible compared to D), the value of horizontal velocity V , preserved during the whole flight, is precisely deduced from the time-of-flight for each detection event. In the following, we measure time of evolution t as run horizontal

distance $x = Vt$ and use a standard value $V_0 = 1 \text{ m s}^{-1}$ of V for fixing numbers and plots.

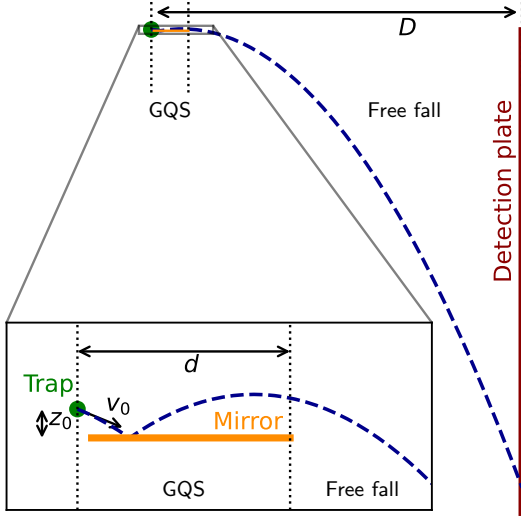


FIG. 1. Schematic representation of the experimental setup. A Gaussian wave-packet is prepared in a trap, and it falls down onto a mirror where it experiences a single bounce. Subsequent free fall reveals interferences which are recorded as positions of atoms on a detection plate.

The important parameters for the initial Gaussian wave-function are the mean altitude z_0 measured above the mirror plate (lying at $z = 0$), the mean vertical velocity v_0 and the altitude dispersion σ_z . The latter is fixed by the harmonic trap frequency f_0 and it determines velocity dispersion through the Heisenberg relation $\sigma_v = \frac{\hbar}{2m\sigma_z}$. The numbers used below are $z_0 = 1 \text{ mm}$, $v_0 = -91.5 \text{ mm s}^{-1}$, and $\sigma_x = 0.4 \text{ }\mu\text{m}$ which corresponds to numbers matching the GBAR experiment with $f_0 = 30 \text{ kHz}$ [35] and $m \sim 1$ atomic mass unit.

The first phase of evolution of the wave-function corresponds to the left-hand side on Figure 1. It starts at initial time $t_0 = 0$ and includes the bounce over the mirror and the free fall before and after it, till the end of the mirror at $x = d$. This evolution is decomposed over the GQS which solve Schrödinger equation in presence of gravity and reflection (assumed perfect at this stage)

$$\psi_t(z) = \sum_n c_n \chi_n(z) e^{-i \frac{E_n t}{\hbar}} \quad , \quad 0 < Vt < d. \quad (1)$$

The eigen-functions $\chi_n(z)$ are Airy functions corresponding to energies E_n . The coefficients c_n are defined so that the expression (1) reproduces the initial Gaussian wave-function $\psi_0(z) = \sum_n c_n \chi_n(z)$. They are given by an analytical expression when the probability of presence at negative altitudes is negligible, which is a very good ap-

proximation for our calculations

$$c_n = \frac{(8\pi)^{\frac{1}{4}}}{\text{Ai}'(-\lambda_n)} \sqrt{\frac{\sigma_z}{\ell_g}} \text{Ai} \left(\frac{z_0}{\ell_g} - \lambda_n + \frac{i v_0 \sigma_z^2}{v_g \ell_g^2} + \frac{\sigma_z^4}{\ell_g^4} \right) \\ \times \exp \left(\frac{\sigma_z^2}{\ell_g^2} \left(\frac{z_0}{\ell_g} - \lambda_n + \frac{i v_0 \sigma_z^2}{v_g \ell_g^2} - \frac{v_0^2}{4v_g^2} + \frac{2\sigma_z^4}{3\ell_g^4} \right) \right), \quad (2) \\ v_g = \sqrt[3]{\frac{2\hbar g}{m}} \quad , \quad \ell_g = \frac{\hbar}{mv_g} \quad , \quad e_g = \frac{mv_g^2}{2}.$$

Relations have been written with quantities reduced to the natural units (v_g, ℓ_g, e_g) for the GQS, and λ_n is the absolute value of the n -th zero of the Ai-function (energies given by $E_n = e_g \lambda_n$).

The second phase of the evolution corresponds to the right-hand side on Figure 1. It starts at the end of the mirror (at $Vt = d$) and lasts till the detection plate (at $Vt = D$). It is described by the quantum propagator which is known for quantum free fall in a constant gravity field. We write the propagator in momentum representation, so that integrals can be done by fast Fourier transforms with considerably reduced computation time

$$\tilde{\psi}_d(p) = \int \psi_d(z) \exp \left(-\frac{i p z}{\hbar} \right) \frac{dz}{\sqrt{2\pi\hbar}}, \\ \tilde{\psi}_D(p) = \tilde{\psi}_d(p + mgT) \\ \times \exp \left(\frac{-iT}{\hbar} \left(\frac{p^2}{2m} + \frac{gpT}{2} + \frac{mg^2T^2}{6} \right) \right), \quad (3) \\ \psi_D(z) = \int \tilde{\psi}_D(p) \exp \left(\frac{i p z}{\hbar} \right) \frac{dp}{\sqrt{2\pi\hbar}}, \\ T = \frac{D - d}{V}.$$

At arrival on the detection plate, the position of the antihydrogen atom is measured with a distribution proportional to the altitude-dependent density of probability $|\psi_D(z)|^2$. The choice of a vertical plate is made for simplifying the presentation of results. Essentially identical results would be obtained for another orientation of the plate by adding details on the final stage of the evolution. In GBAR, the free fall chamber will be equipped with detectors installed on all surfaces, vertical and horizontal and the dedicated analysis will have to be adapted to the real geometrical configuration.

Numbers for the plots shown below are $d = 30 \text{ mm}$ for the horizontal distance from the source to the end of mirror and $D = 300 \text{ mm}$ from the source to the detection plate. These numbers match the planned geometry for the GBAR experiment. We repeat that horizontal velocity V is measured for each detection event by the time-of-flight. It is supposed that, for all values of V in the horizontal velocity distribution, atoms undergo a single bounce with a probability close to unity.

The results of the calculations of evaluation are gathered on Figure 2 where the altitude-dependent density $|\psi_t(z)|^2$ is presented as a function of run distance $x = Vt$.

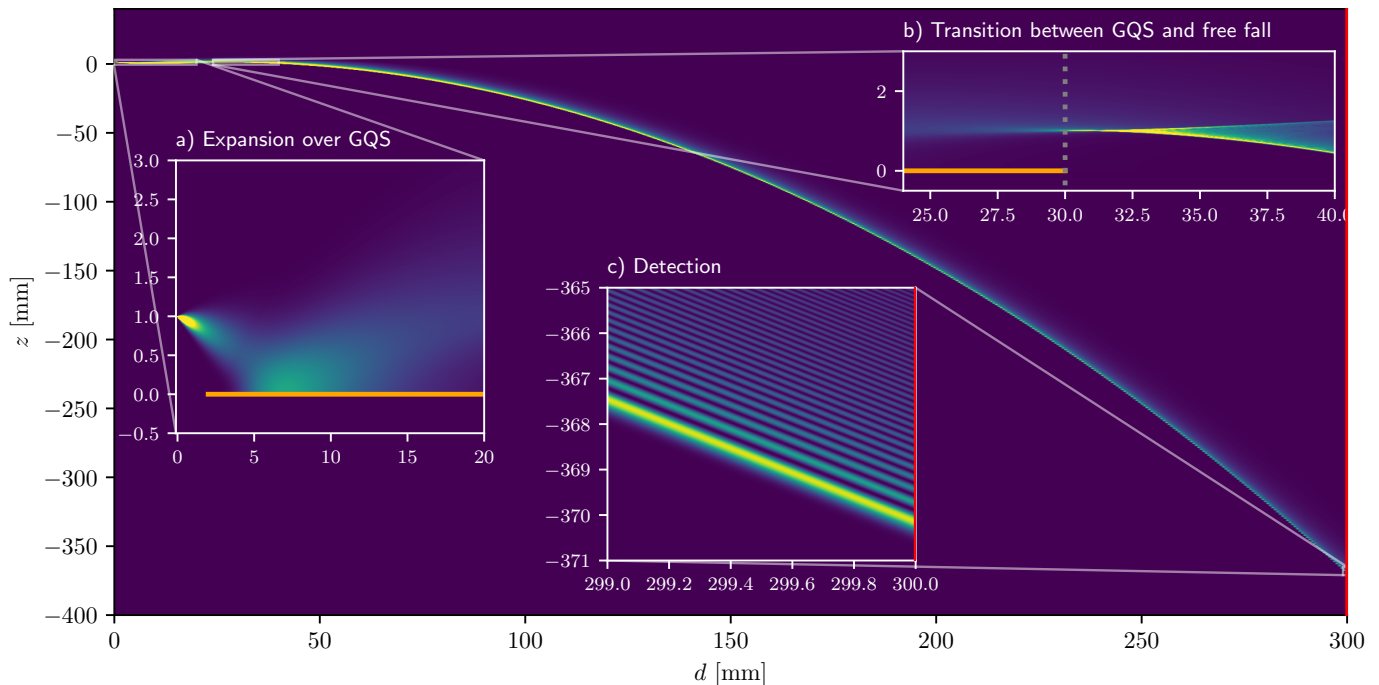


FIG. 2. Representation of the evolution of the wave-function from the source to the detection. The square modulus $|\psi(z)|^2$ of the wave-function is represented as a function of $x = Vt$ (for a velocity $V_0 = 1 \text{ m s}^{-1}$). The main plot shows the mean motion from the source to the detection plate. Details are shown in the zooms devoted to zones of particular interest: a) evolution of the wave-function over the mirror (described by eq.1); b) transition to the second phase corresponding to free fall (described by eq.3); c) fully revealed interference fringes after a long phase of free fall after the mirror.

The main figure represents the global evolution of the density from the source to the bounce and then till the detection plate. Figure 2 also shows zooms on three zones of particular interest. The first zone (a) shows the beginning of the evolution from the source till the middle of mirror, which includes the bounce. As the mean initial altitude z_0 is very large compared to the scale $\ell_g \sim 6 \mu\text{m}$ of GQS, we have made the numerical decomposition of the wave-function over a large number (12 000) of GQS, in order to have an accurate description of wave-functions during this phase. We have chosen the dimensions of the mirror so that all atoms bounce once on it, with the mirror plate ending at 30 mm from the source. This dimension is not critical but it fits our purpose of having nearly all atoms having one bounce. We have also drawn a mirror plate beginning at 2 mm of the source, which does not change the idea but would make easier the insertion of the mirror in the planned free fall chamber for GBAR.

The second zone (b) shows the transition from the first phase to the second one around the size of the mirror. After this point, we see interferences beginning to appear in the probability distribution. The third zone (c) shows well formed interference fringes fully revealed after a free fall during a time longer than that of the two first zones. These fringes depend on the free fall acceleration, which will lead to the accuracy of the measurement of g dis-

cussed in the following.

One may emphasize at this point that the interferences are not produced by the superposition of two waves having followed widely separated classical trajectories, as would be the case for usual matter-wave gravimeters. In other words, there is no beam splitting in this concept of interferometer and all quantum paths originate from a unique cell in phase space corresponding to the Heisenberg-limited initial wave-packet.

At the end of this discussion of evaluation, we get the altitude-dependent probability density on the vertical detection plate, that is $|\psi_D(z)|^2$ shown on Figure 3. The full blue curve has been calculated for the case $g = g_0$ where $g_0 = 9.81 \text{ m s}^{-2}$ is the standard gravity acceleration at Earth surface. It shows neat interference fringes with an extremely good contrast (the curve goes to zero repeatedly when the altitude is varied). The other curves correspond to slightly different values of g with relative variations of 10^{-4} . These two curves are modified essentially through a shift towards the right and left sides respectively for lower and higher values of g . There shifts are highly visible for the slight changes considered in the calculations, and this already shows that the accuracy should be much better than 10^{-4} , even with limited samples of detected events.

The expected accuracy is quantitatively evaluated now

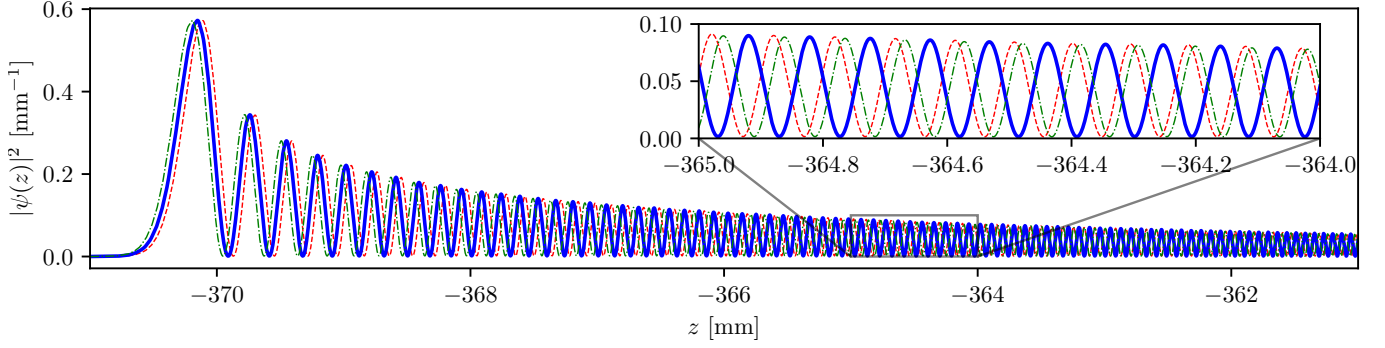


FIG. 3. Three curves for the probability of detection at altitude z calculated for slightly different values of g . The solid (blue) curve corresponds to the standard gravity acceleration, while the dashed (red, shifted towards the right) and dotted (green, shifted towards the left) curves correspond respectively to values decreased and increased by a relative variations of 10^{-4} . The zoom shows that fringes are visible on a large range of values of z . (colors online)

by using the simulation technique proposed in [28]. In a first step, data mimicking the results of a forthcoming experiment are produced by randomly drawing N events from the curve calculated for the standard value g_0 of the free fall acceleration. These points are then seen as a sample of N detection events in the experiment and a data analysis is simulated with a maximum likelihood statistical method. Each drawing of a sample of N data points gives an estimator \hat{g} defined as the argument maximizing the log-likelihood function. We finally repeat this numerical simulations M times and draw an histogram of the obtained estimators \hat{g} .

We show on the top part of Figure 4 the normalised histograms calculated for a large number $M = 40000$ of repeated simulations, with the numbers $N = 100$ and $N = 1000$ of data points mimicking an experiment. For a large enough sample size N , the histogram tends to a Gaussian distribution and the expected experimental accuracy can be predicted as the dispersion σ_g of the distribution of estimators provided the uncertainties are dominated by statistical sampling of data. For the number $N = 1000$ corresponding to the planned number of detection events in GBAR, we find an expected relative accuracy σ_g/g_0 of 1.0×10^{-6} which is better by roughly 4 orders of magnitude than for the classical timing experiment, with the same number of detection events. It is even better than what was found in [28] for a quantum interference with many bounces although we have considered here a single-bounce scheme.

Finally we plot the variation of the expected relative accuracy σ_g/g_0 versus the sample size N on the bottom part of Figure 4. The blue dots are the values obtained from our simulation procedure for values of N ranging to $N = 1000$ to the small sample size $N = 50$. For large enough values of N , the expected accuracies vary according to the Cramer-Rao law [36–38], shown as the dashed red line on the figure. The latter is fixed by the Fisher information $\mathcal{I}_{\mathcal{F}}$ which can be calculated from the

dependence of the signal to the parameter

$$\frac{\sigma_{\text{CR}}}{g_0} = \frac{1}{\sqrt{N \mathcal{I}_{\mathcal{F}}}} \quad , \quad \mathcal{I}_{\mathcal{F}} = g_0^2 \int \frac{(\partial_g |\psi_g(z)|^2)^2}{|\psi_g(z)|^2} dz. \quad (4)$$

This means that the statistical efficiency of the measurement is thus good. For the values of parameters given

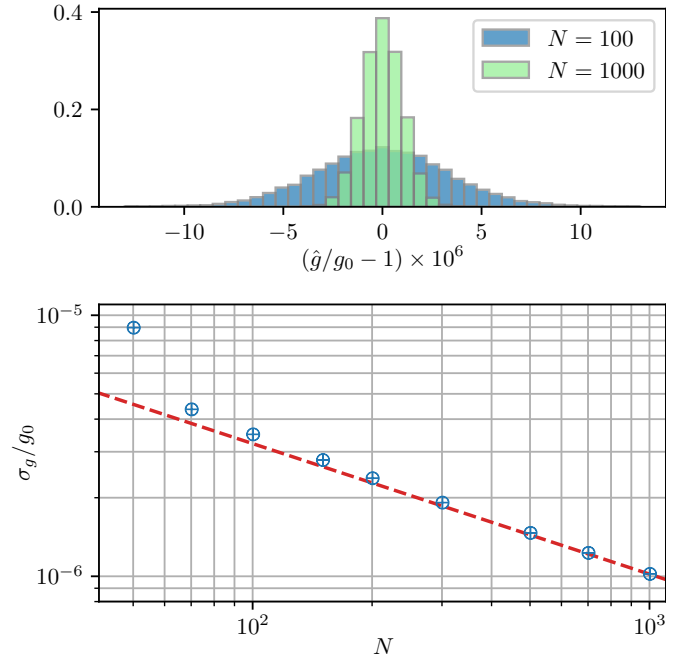


FIG. 4. Top plot : Histograms of the estimators \hat{g} for a large number of simulations performed each with N randomly drawn detection events. The broader blue histogram corresponds to $N = 100$ and the narrower green one to $N = 1000$. Bottom plot : Expected relative accuracy σ_g/g_0 for the measurement of g calculated from the dispersion on histograms, and represented as blue dots depending on the number N . For large enough values of N , the dots are aligned on the dashed red line showing the Cramer-Rao law. (colors online)

above, we numerically estimate the Fisher information to $\sim 1 \times 10^9$, which for $N = 1000$ gives an expected relative precision $\sim 1.0 \times 10^{-6}$. For lower values of N , the simulated relative accuracy σ_g/g_0 is as expected above the Cramer-Rao law. For example, the simulated value is a factor 2 larger than the Cramer-Rao bound for $N = 50$. A measurement with such an undersampled number of events goes out of the domain of applicability of common statistical techniques based on Gaussian laws. We however emphasize that adapted techniques would allow one to approach relative accuracies of the order of 10^{-5} which would still be better than classical experiment by 3 orders of magnitude.

The agreement of the results of simulation techniques with the Cramer-Rao law is a good hint of robustness of simulations (for $N > 100$). Calculations based on the Fisher information are easier to perform and they can be used to explore variation of accuracy with parameters. We have used the method to choose the parameter v_0 once z_0 and σ_z were chosen from considerations related to GBAR experiment. It is also easy to prove in this way that the expected accuracy would be improved by increasing the free fall height before the mirror (z_0 larger) as well as after the mirror (D larger), in full conformity with classical expectations for a free fall experiment. The free fall height after the bounce is limited by the size of free fall chamber in the experiment, and our choice above matches the plans for the GBAR experiment.

In order to discuss the effect of a variation of z_0 , we have to be more precise on the probability of quantum reflection, as it depends on the incidence energy and the specific material constituting the mirror plate [24, 25]. The probability of annihilation was very small for the low energies considered in [28, 29] but its importance was amplified by the large number of bounces needed to get a good accuracy there. In the new concept proposed in this letter, incidence energy is higher on the mirror, so that quantum reflection probability is farther from 1, but there is only one bounce. Numbers given above for z_0 and v_0 lead to a reflection probability of $\sim 87\%$ on a bulk silica plate [24] and of $\sim 97.5\%$ on a thick film of liquid ^4He [25]. Non reflected antihydrogen atoms are annihilated on the mirror and they are lost for our signal which requires the subsequent free fall evolution. This means that the number of detected events is reduced by approximately $\sim 13\%$ when the mirror is made of silica, $\sim 2.5\%$ for a thick film of liquid helium, with these numbers to be taken into account in the accuracy analysis presented above. One note also that atoms may be quantum reflected on the detection plate instead of being annihilated there and that this loss in the number of detection events has also to be taken into account. This problem was already present for the classical GBAR experiment and all relevant numbers can be found in [24].

As quantum reflection is not perfect, it depends on energy and this has to be included in the data analysis to

avoid possible systematic errors when the experiment will be performed. The treatment will be based on the calculations of quantum reflection amplitude resulting from Casimir-Polder interaction, for example on a silica plate [39]. With the single-bounce interference technique, this will be done more easily than for a many-bounce experiment, so that the measurement of g will be made more accurate and reliable than with two previous proposals.

The spatial resolution on the detection plate will also be a critical argument for an experimental implementation of the new scheme. It is indeed important to collect information on a large enough fraction of fringes in the interference pattern on Figure 3 to reach the accuracy discussed above. It has to be noted at this point that antimatter detectors with submicrometer resolution have recently been validated and will be further developed for future antihydrogen gravity measurements [40].

In this letter, we have proposed and studied a new concept of interferometer which differs from the known configurations for matter-wave gravimeters, where two waves interfere after beam splitters and propagations along separated classical trajectories. We have used the improvement of accuracy in the GBAR experiment to specify numbers and expected performance of the new concept, and this has led to an improvement of about 4 orders of magnitude for the measurement of free fall acceleration of antihydrogen, using the same resource in terms of number and initial state for $\bar{\text{H}}$ atoms. The concept is not restricted to this application and it may open new ways of investigating gravitational properties of rare or exotic species, with particular interest when the sample size for detection events or the time available for measurement are limited for intrinsic physical reasons.

We thank our colleagues in the GBAR collaboration <https://gbar.web.cern.ch/> and GRASIAN collaboration <https://grasian.eu/> for insightful discussions, in particular S. Baessler, C. Blondel, P. P. Blumer, C. Christen, P.-P. Crepin, P. Crivelli, P. Debu, A. Douillet, C. Drag, N. Garroum, R. Guérout, L. Hilico, P. Indelicato, G. Janka, J.-P. Karr, S. Guellati-Khelifa, L. Liskay, B. Mansoulié, V. V. Nesvizhevsky, F. Nez, N. Paul, P. Pérez, J. Piquinto, C. Regenfus, O. Rousselle, F. Schmidt-Kaler, K. Schreiner, A. Yu. Voronin, S. Wolf, P. Yzombard. This work was supported by the Programme National GRAM of CNRS/INSU with INP and IN2P3 co-funded by CNES, and by Agence Nationale pour la Recherche, Photoplus project Nr. ANR 21-CE30-0047-01. Joachim Guyomard was supported by QuantEdu-France (ANR-22-CMAS-0001) in the framework of France 2030.

* joachim.guyomard@lkb.upmc.fr

† pierre.clade@lkb.upmc.fr

‡ serge.reynaud@lkb.upmc.fr

- [1] E. K. Anderson, C. J. Baker, W. Bertsche, N. M. Bhatt, G. Bonomi, A. Capra, I. Carli, C. L. Cesar, M. Charlton, A. Christensen, et al. Observation of the effect of gravity on the motion of antimatter. *Nature*, 621:716–722, 2023.
- [2] C. M. Will. The confrontation between general relativity and experiment. *Living Reviews in Relativity*, 17:1–117, 2014.
- [3] T. A. Wagner, S. Schlamminger, J. H. Gundlach, and E. G. Adelberger. Torsion-balance tests of the weak equivalence principle. *Classical and Quantum Gravity*, 29:184002, 2012.
- [4] V. Viswanathan, A. Fienga, O. Minazzoli, L. Bernus, J. Laskar, and M. Gastineau. The new lunar ephemeris INPOP17a and its application to fundamental physics. *Monthly Notices of the Royal Astronomical Society*, 476:1877–1888, 2018.
- [5] P. Touboul, G. Métris, M. Rodrigues, J. Berge, A. Robert, Q. Baghi, Y. André, J. Bedouet, D. Boulanger, S. Bremer, P. Carle, R. Chhun, B. Christophe, V. Cipolla, T. Damour, P. Danto, L. Demange, H. Dittus, O. Dhuicque, P. Fayet, B. Foulon, P.-Y. Guidotti, D. Hagedorn, E. Hardy, P.-A. Huynh, P. Kayser, S. Lala, C. Laemmerzahl, V. Lebat, F. Liorzou, M. List, F. Loeffler, I. Panet, M. Pernot-Borras, L. Perraud, S. Pires, B. Pouilloux, P. Prieur, A. Rebray, S. Reynaud, B. Rievers, H. Selig, L. Serron, T. Sumner, N. Tanguy, P. Torresi, and P. Visser. MICROSCOPE mission: Final results of the test of the equivalence principle. *Physical Review Letters*, 129:121102, 2022.
- [6] P. Touboul, G. Métris, M. Rodrigues, J. Bergé, A. Robert, Q. Baghi, Y. André, J. Bedouet, D. Boulanger, S. Bremer, P. Carle, R. Chhun, B. Christophe, V. Cipolla, T. Damour, P. Danto, L. Demange, H. Dittus, O. Dhuicque, P. Fayet, B. Foulon, P.-Y. Guidotti, D. Hagedorn, E. Hardy, P.-A. Huynh, P. Kayser, S. Lala, C. Laemmerzahl, V. Lebat, F. Liorzou, M. List, F. Loeffler, I. Panet, M. Pernot-Borras, L. Perraud, S. Pires, B. Pouilloux, P. Prieur, A. Rebray, S. Reynaud, B. Rievers, H. Selig, L. Serron, T. Sumner, N. Tanguy, P. Torresi, and P. Visser. Result of the MICROSCOPE weak equivalence principle test. *Classical and Quantum Gravity*, 39(20), 2022.
- [7] E. Kajari, N. L. Harshman, E. M. Rasel, S. Stenholm, G. Süssmann, and W. P. Schleich. Inertial and gravitational mass in quantum mechanics. *Applied Physics B*, 100:43–60, 2010.
- [8] S. Herrmann, H. Dittus, C. Lämmerzahl, (for the QUANTUS and PRIMUS teams). Testing the equivalence principle with atomic interferometry. *Classical and Quantum Gravity*, 29:184003, 2012.
- [9] B. Barrett, L. Antoni-Micollier, L. Chichet, B. Battelier, P. A. Gominet, A. Bertoldi, P. Bouyer, and A. Landragin. Correlative methods for dual-species quantum tests of the weak equivalence principle. *New Journal of Physics*, 17:085010, 2015.
- [10] P. Asenbaum, C. Overstreet, M. Kim, J. Curti, and M. A. Kasevich. Atom-interferometric test of the equivalence principle at the 10^{-12} level. *Physical Review Letters*, 125:191101, 2020.
- [11] G. M. Tino, L. Cacciapuoti, S. Capozziello, G. Lambiase, and F. Sorrentino. Precision gravity tests and the Einstein Equivalence Principle. *Progress in Particle and Nuclear Physics*, 112:103772, 2020.
- [12] F. M. Huber, R. A. Lewis, E. W. Messerschmid, and G. A. Smith. Precision tests of Einstein’s Weak Equivalence Principle for antimatter. *Advances in Space Research*, 25:1245 – 1249, 2000.
- [13] W. A. Bertsche, E. Butler, M. Charlton, and N. Madsen. Physics with antihydrogen. *Journal of Physics B: Atomic, Molecular and Optical Physics*, 48:232001, 2015.
- [14] W. A. Bertsche. Prospects for comparison of matter and antimatter gravitation with alpha-g. *Philosophical Transactions of the Royal Society A: Mathematical, Physical and Engineering Sciences*, 376:20170265, 2018.
- [15] Y. Yamazaki. Cold and stable antimatter for fundamental physics. *Proceedings of the Japan Academy, Series B*, 96:471–501, 2020.
- [16] P. Indelicato, G. Chardin, P. Grandemange, D. Lunney, V. Manea, A. Badertscher, P. Crivelli, A. Curioni, A. Marchionni, B. Rossi, A. Rubbia, V. Nesvizhevsky, D. Brook-Roberge, P. Comini, P. Debu, P. Dupré, L. Liskay, B. Mansoulié, P. Pérez, J.-M. Rey, B. Raymond, N. Ruiz, Y. Sacquin, B. Vallage, F. Biraben, P. Cladé, A. Douillet, G. Dufour, S. Guellati, L. Hilico, A. Lambrecht, R. Guérout, J.-P. Karr, F. Nez, S. Reynaud, C. I. Szabo, V.-Q. Tran, J. Trapateau, A. Mohri, Y. Yamazaki, M. Charlton, S. Eriksson, N. Madsen, D. P. van der Werf, N. Kuroda, H. Torii, Y. Nagashima, F. Schmidt-Kaler, J. Walz, S. Wolf, P.-A. Hervieux, G. Manfredi, A. Voronin, P. Froelich, S. Wronka, and M. Staszczak. The GBAR project, or how does antimatter fall? *Hyperfine Interactions*, 228:141–150, 2014.
- [17] P. Pérez, D. Banerjee, F. Biraben, D. Brook-Roberge, M. Charlton, P. Cladé, P. Comini, P. Crivelli, O. Dalkarov, P. Debu, A. Douillet, G. Dufour, P. Dupré, S. Eriksson, P. Froelich, P. Grandemange, S. Guellati, R. Guérout, J. M. Heinrich, P.-A. Hervieux, L. Hilico, A. Husson, P. Indelicato, S. Jonsell, J.-P. Karr, K. Khabarova, N. Kolachevsky, N. Kuroda, A. Lambrecht, A. M. M. Leite, L. Liskay, D. Lunney, N. Madsen, G. Manfredi, B. Mansoulié, Y. Matsuda, A. Mohri, T. Mortensen, Y. Nagashima, V. Nesvizhevsky, F. Nez, C. Regenfus, J.-M. Rey, J.-M. Raymond, S. Reynaud, A. Rubbia, Y. Sacquin, F. Schmidt-Kaler, N. Sillitoe, M. Staszczak, C. I. Szabo-Foster, H. Torii, B. Vallage, M. Valdes, D. P. Van der Werf, A. Voronin, J. Walz, S. Wolf, S. Wronka, and Y. Yamazaki. The GBAR antimatter gravity experiment. *Hyperfine Interactions*, 233:21, 2015.
- [18] P. Adrich, P. Blumer, G. Caratsch, M. Chung, P. Cladé, P. Comini, P. Crivelli, O. Dalkarov, P. Debu, A. Douillet, D. Drapier, P. Froelich, N. Garroum, S. Guellati-Khelifa, J. Guyomard, P.-A. Hervieux, L. Hilico, P. Indelicato, S. Jonsell, J.-P. Karr, B. Kim, S. Kim, E.-S. Kim, Y. J. Ko, T. Kosinski, N. Kuroda, B. M. Latacz, B. Lee, H. Lee, J. Lee, E. Lim, L. Liskay, D. Lunney, G. Manfredi, B. Mansoulié, M. Matusiak, V. Nesvizhevsky, F. Nez, S. Niang, B. Ohayon, K. Park, N. Paul, P. Pérez, C. Regenfus, S. Reynaud, C. Roumegoux, J.-Y. Roussé, Y. Sacquin, G. Sadowski, J. Sarkisyan, M. Sato, F. Schmidt-Kaler, M. Staszczak, K. Szymczyk, T. A. Tanaka, B. Tuchming, B. Vallage, A. Voronin, D. P. van der Werf, A. Welker, D. Won, S. Wronka, Y. Yamazaki, K.-H. Yoo, and P. Yzombard. Production of antihydrogen atoms by 6 keV antiprotons through a positronium cloud. *The European Physical Journal C*, 83:1004, 2023.
- [19] F. Shimizu. Specular reflection of very slow metastable

- neon atoms from a solid surface. *Physical Review Letters*, 86:987–990, 2001.
- [20] V. Druzhinina and M. De Kieviet. Experimental observation of quantum reflection far from threshold. *Physical Review Letters*, 91:193202, 2003.
- [21] H. Oberst, Y. Tashiro, K. Shimizu, and F. Shimizu. Quantum reflection of He^* on silicon. *Physical Review A*, 71:052901, 2005.
- [22] T. A. Pasquini, M. Saba, G.-B. Jo, Y. Shin, W. Ketterle, D. E. Pritchard, T. A. Savas, and N. Mulders. Low velocity quantum reflection of Bose-Einstein condensates. *Physical Review Letters*, 97:093201, 2006.
- [23] A. Yu Voronin and P. Froelich. Quantum reflection of ultracold antihydrogen from a solid surface. *Journal of Physics B*, 38:L301, 2005.
- [24] G. Dufour, A. Gérardin, R. Guérout, A. Lambrecht, V. V. Nesvizhevsky, S. Reynaud, and A. Yu. Voronin. Quantum reflection of antihydrogen from the Casimir potential above matter slabs. *Physical Review A*, 87:012901, 2013.
- [25] P.-P. Crépin, E. A. Kupriyanova, R. Guérout, A. Lambrecht, V. V. Nesvizhevsky, S. Reynaud, S. Vasilyev, and A. Yu. Voronin. Quantum reflection of antihydrogen from a liquid helium film. *EPL (Europhysics Letters)*, 119:33001, 2017.
- [26] V. V. Nesvizhevsky, H. G. Börner, A. K. Petukhov, H. Abele, S. Baessler, F. J. Rueß, T. Stöferle, A. Westphal, A. M. Gagarski, G. A. Petrov, and A. V. Strelkov. Quantum states of neutrons in the Earth’s gravitational field. *Nature*, 415:297–299, 2002.
- [27] V. V. Nesvizhevsky, A. Yu. Voronin, R. Cubitt, and K. V. Protasov. Neutron whispering gallery. *Nature Physics*, 6:114, 2009.
- [28] P.-P. Crépin, C. Christen, R. Guérout, V. V. Nesvizhevsky, A. Yu. Voronin, and S. Reynaud. Quantum interference test of the equivalence principle on antihydrogen. *Physical Review A*, 99:042119, 2019.
- [29] O. Rousselle, P. Cladé, S. Guellati-Khelifa, R. Guérout, and S. Reynaud. Quantum interference measurement of the free fall of anti-hydrogen. *European Physical Journal D*, 76:209, 2022.
- [30] Mark Kasevich and Steven Chu. Atomic interferometry using stimulated Raman transitions. *Physical Review Letters*, 67:181–184, 1991.
- [31] P. Storey and C. Cohen-Tannoudji. The Feynman path integral approach to atomic interferometry. A tutorial. *J. Phys. II France*, 4:1999–2027, 1994.
- [32] C. J. Bordé. Theoretical tools for atom optics and interferometry. *Comptes Rendus de l’Académie des Sciences - Series IV - Physics*, 2:509–530, 2001.
- [33] P. Gillot, O. Francis, A. Landragin, F. Pereira dos Santos, and S. Merlet. Stability comparison of two absolute gravimeters: Optical versus atomic interferometers. *Metrologia*, 51:L15, 2014.
- [34] J. Walz and T. W. Hänsch. A proposal to measure anti-matter gravity using ultracold antihydrogen atoms. *General Relativity and Gravitation*, 36:561–570, 2004.
- [35] L. Hilico, J.-P. Karr, A. Douillet, P. Indelicato, S. Wolf, and F. Schmidt-Kaler. Preparing single ultra-cold antihydrogen atoms for free-fall in GBAR. *International Journal of Modern Physics Conference Series*, 30:1460269, 2014.
- [36] M. Fréchet. Sur l’extension de certaines évaluations statistiques au cas de petits échantillons. *Revue de l’Institut International de Statistique / Review of the International Statistical Institute*, 11:182–205, 1943.
- [37] H. Cramér. *Mathematical Methods of Statistics*. Princeton Landmarks in Mathematics PMS-9. Princeton University Press, 1946.
- [38] P. Réfrégier. *Noise Theory and Application to Physics*. Advanced Texts in Physics. Springer, 2004.
- [39] P.-P. Crépin, R. Guérout, and S. Reynaud. Improved effective range expansion for Casimir-Polder potential. *European Physical Journal D*, 73:256, 2019.
- [40] M. Berghold, D. Orsucci, F. Guatieri, S. Alfaro, M. Auzins, B. Bergmann, P. Burian, R. S. Brusa, A. Camper, R. Caravita, et al. Real-time antiproton annihilation vertexing with submicrometer resolution. *Science Advances*, 11:eads1176, 2025.